# MODEL PREDICTIVE CONTROL BASED APPROACH TO TRAJECTORY OPTIMIZATION OF AUTONOMOUS UNDERWATER VEHICLES

**A THESIS**

*submitted in partial fulfillment of the requirements*

*for the award of the dual degree of*

**Bachelor of Science-Master of Science**

*in*

**PHYSICS**

*by*

**SARTHAK MISHRA**

**(18388)**


**DEPARTMENT OF PHYSICS**
**INDIAN INSTITUTE OF SCIENCE EDUCATION AND RESEARCH BHOPAL**
**BHOPAL - 462066**
**April 2023**

(This page is intentionally left blank)

भारतीय विज्ञान शिक्षा एवं अनुसंधान संस्थान भोपाल
Indian Institute of Science Education and Research
Bhopal
(Estb. By MHRD, Govt. of India)

# CERTIFICATE

This is to certify that **Sarthak Mishra**, BS-MS (Physics), has worked on the project entitled **'Model Predictive Control based approach to Trajectory Optimization of Autonomous Underwater Vehicles'** under my supervision and guidance. The content of this report is original and has not been submitted elsewhere for the award of any academic or professional degree.

Assinado por : **JOÃO TASSO DE FIGUEIREDO BORGES DE SOUSA**
Num. de Identificação: 05476909
Data: 2023.05.01 17:52:50+01'00'

CARTÃO DE CIDADÃO

**Dr. Sujit P B**

**April 2023**
**IISER Bhopal**

| Committee Member | Signature | Date |
|---|---|---|
| | | |
| | | |
| | | |

# ACADEMIC INTEGRITY AND COPYRIGHT DISCLAIMER

I hereby declare that this project is my own work and, to the best of my knowledge, it contains no materials previously published or written by another person, or substantial proportions of material which have been accepted for the award of any other degree or diploma at IISER Bhopal or any other educational institution, except where due acknowledgement is made in the document.

I certify that all copyrighted material incorporated into this document is in compliance with the Indian Copyright Act (1957) and that I have received written permission from the copyright owners for my use of their work, which is beyond the scope of the law. I agree to indemnify and save harmless IISER Bhopal from any and all claims that may be asserted or that may arise from any copyright violation.

**April 2023** **Sarthak Mishra**
**IISER Bhopal**

# ACKNOWLEDGEMENT

I would like to express my heartfelt appreciation to every individual who have played a significant role throughout my academic journey.

First and foremost, I am grateful to my grandfather, Mr Kashi Prasad Mishra, for instilling in me the virtues of honesty and truthfulness, which have played a significant role in shaping my character. I also extend my gratitude to my parents, Mr Bidhu Bhusan Mishra and Mrs Sanghamitra Sarangi, my sister, Sinu, and my aunts, Runu Nani and Jhunu Nani, for their unwavering love, encouragement, and support.

I am deeply thankful to my advisor, Prof. João Borges de Sousa, for providing me with the opportunity to conduct research under his guidance. Also, I am grateful to my guide, Dr Renato Mendes, for his crucial ideas and suggestions throughout my thesis journey, which has been invaluable in shaping my research.

I would also like to thank Dr. P. B. Sujit for his consistent support and availability. The innovative ideas shared by him have been invaluable in exploring diverse dimensions of my research. Additionally, the thought-provoking discussions, and valuable suggestions shared by my colleagues at Moonlab have played a vital role in my growth as a researcher.

Lastly, I want to express my heartfelt gratitude to my dearest friends - Kaibalya, Abhisek, Soumya, and Kshirabdhee, who have always been there for me through thick and thin. I am also immensely thankful to Srinibash, Subhasish, Siddhant, Nikita, Saima, Afreen, Uttara, Sreevathsa, and many others for being a constant source of positive energy and inspiration for me. Your encouragement and uplifting conversations have helped me navigate through some of the toughest times of my life.

I am deeply grateful for the love and support of everyone who has contributed to my thesis journey. Your presence has made this journey all the more memorable and worthwhile. Thank you.

**Sarthak Mishra**

# ABSTRACT

This study presents the application of Model Predictive Control (MPC) for the optimal trajectory optimization of a six-degree-of-freedom (DOF) REMUS 100 Autonomous Underwater Vehicle (AUV). The MPC approach provides a control strategy that allows for the real-time adjustment of the vehicle's trajectory, considering current measurements and constraints. The MPC controller is designed using a mathematical model of the vehicle's dynamics, and the optimization problem is formulated to minimize the tracking error of the desired trajectory.

Simulation results demonstrate the effectiveness of the proposed approach in generating an optimal trajectory for the underwater vehicle. The approach provides accurate tracking of the desired trajectory while ensuring that the vehicle remains within operational constraints. The results indicate that the MPC approach can effectively control the underwater vehicle's motion, even in the presence of disturbances and uncertainties. The proposed approach is a promising strategy for the optimal trajectory optimization of underwater vehicles, which is useful for applications such as underwater exploration, oceanography, and marine transportation.

In conclusion, the study demonstrates that the MPC-based approach can achieve optimal trajectory optimization of underwater vehicle in real-time while meeting operational constraints. The approach can be further developed to incorporate more complex constraints and objectives to enhance the performance of underwater vehicles in various applications.

# LIST OF SYMBOLS OR ABBREVIATIONS

| | |
|---|---|
| $\eta$ | Position and orientation of the vehicle with respect to the inertial or earth-fixed reference frame |
| $v$ | Translational and rotational velocities of the vehicle with respect to the body-fixed reference frame |
| $M$ | Total Inertial Mass Matrix |
| $C(v)$ | Total Non-Inertial Force and Moment matrix |
| $D(v)$ | Damping Force matrix |
| $g(v)$ | Restoring Force matrix |
| $\tau$ | Total Force and Moment acting on the vehicle |
| $T_1(\eta_1)$ | Position transformation matrix from body-fixed reference frame to earth-fixed reference frame |
| $T_2(\eta_2)$ | Rotational transformation matrix from body-fixed reference frame to earth-fixed reference frame |
| DOF | Degrees of Freedom |
| REMUS | Remote Environment Monitoring UnitS |
| CG | Centre of Gravity |
| CB | Centre of Buoyancy |
| AUV | Autonomous Underwater Vehicle |
| MPC | Model Predictive Control |

# List of Figures

# List of Tables

# Contents

# Chapter 1

# Introduction

## 1.1 Motivation

The field of autonomous underwater vehicles (AUVs) has seen significant advancements in recent years, with applications ranging from marine science to underwater inspection and exploration [1]. However, the effective and efficient control of AUVs remains a challenge. The motivation behind choosing this topic as master's thesis is to develop an optimal trajectory control system for a 6 Degrees-of-Freedom (DOF) AUV using model predictive control (MPC) to enhance the vehicle's motion control capabilities [2]. The study will focus on the design and implementation of an MPC-based control system that can optimize the AUV's trajectory while taking into account various constraints such as actuator limits and collision avoidance [3]. The system's performance will be evaluated through simulations and experiments in a controlled environment [4]. The results of this study have the potential to contribute to the development of more efficient and reliable AUVs, which can play a vital role in underwater applications [5]. Overall, this master's thesis seeks to enhance the understanding of the potential of MPC-based trajectory control systems to improve the performance of AUVs and contribute to the field of underwater robotics [6].

## 1.2 Basic Introduction

Autonomous Underwater Vehicles (AUVs) have emerged as essential tools for ocean exploration, environmental monitoring, and resource exploration in deep-sea environments [3]. One of the most critical challenges in AUVs operation is to accurately control their trajectory to accomplish a specific task or mission [7]. In this context, Model Predictive Control (MPC) has emerged as a powerful technique to optimize AUVs trajectory and improve their performance [6]. The six degrees of freedom (6DOF) autonomous underwater vehicle (AUV) trajectory optimization using MPC involves using a mathematical model of the AUV's dynamics to predict the future states of the system and generate optimal control actions [8]. The MPC algorithm is designed to account for the system constraints, such as the AUV's physical limitations and environmental disturbances, to ensure that the vehicle follows the desired trajectory accurately [9]. This approach has proven effective in optimizing the AUV's trajectory for a wide range of applications, including seabed mapping, underwater inspection, and scientific research.

This study aims to understand the control of autonomous vehicles for underwater service and model the same with the help of a simulator. A Newton-Euler approach for the derivation of the 6 DOF equations of motion is carried out [10]. Unmanned Underwater Vehicles (UUVs) derive their propulsive and maneuvering forces from interaction with the ocean water, so hydro static and hydrodynamic forces play a major role in deriving the trajectories [11]. In this model, the equations for these forces have been evaluated for drag and lift from body and control surfaces [7]. The control model is required to traverse the best possible trajectory in order to reach the target way point in minimum time elapsed. Model Predictive Control have been used to find the optimal trajectory of the underwater vehicle in constrained systems to accomplish this task [9].

## 1.3 Technical Introduction

Autonomous Underwater Vehicles (AUVs) are unmanned vehicles that operate in the ocean for various tasks such as environmental monitoring, underwater exploration, and resource exploration. AUVs are becoming increasingly popular due to their ability to perform tasks efficiently and without human intervention [12]. However, controlling the trajectory of an AUV is a challenging task, especially in dynamic and uncertain underwater environments [13]. The trajectory optimization of an AUV involves finding the optimal control actions to steer the vehicle along a predefined path to achieve a specific mission objective [14].

Model Predictive Control (MPC) is a widely used control technique that has gained attention in recent years for AUV trajectory optimization. MPC is a predictive control technique that uses a mathematical model of the system to predict future states and optimize control actions. It has been used in various applications such as industrial process control, aerospace, and robotics [9]. MPC provides a systematic approach to optimize the trajectory of an AUV by considering system constraints and disturbances [8].

The motion of an AUV is characterized by 6DOF, which include three translational degrees of freedom (surge, sway, and heave) and three rotational degrees of freedom (roll, pitch, and yaw) [15]. The control of an AUV's 6DOF motion is achieved by applying appropriate control inputs such as thruster forces, rudder angles, and control surface deflections [12]. The MPC algorithm is designed to generate optimal control inputs based on the AUV's mathematical model, which accounts for the dynamics of the vehicle, actuator constraints, and external disturbances [16].

To provide a foundation for the study of maneuvering and motion control of autonomous vehicles, it is necessary to establish certain assumptions and considerations [17]. Some of these assumptions include:

- The vehicle is treated as a rigid body, with no deformation or flexibility considered in the analysis.
- The rotational effects of the earth's rotation are considered negligible

in the vehicle's acceleration components.

- The primary forces acting on the vehicle are of **inertial** and **gravitational** origin. For land-based vehicles, additional **contact forces** between wheels/tracks and the ground must also be considered. For marine vehicles, **hydrostatic**, propulsion, thruster, and **hydrodynamic forces** from lift and drag are also present. For air vehicles, **propulsion**, **lift**, and **drag** forces are the primary contributors.

These assumptions allow for a simplified analysis of the vehicle's motion, while still accounting for the major factors that influence its behavior [14]. By understanding the basic principles of vehicle kinematics, we can design and optimize autonomous vehicle control systems that can effectively navigate and operate in a variety of environments [18].

The mathematical model of an AUV can be developed using various methods such as first-principles modeling, system identification, or data-driven modeling [19]. First-principles modeling involves developing a mathematical model based on the physical laws that govern the AUV's motion. System identification involves identifying the parameters of the mathematical model by fitting it to experimental data [10]. Data-driven modeling involves developing a mathematical model based on the AUV's data, such as sensor measurements, and using machine learning techniques to estimate the model parameters [13].

The MPC algorithm for AUV trajectory optimization involves the following steps:

- **Prediction:** the MPC algorithm uses the mathematical model of the AUV to predict future states of the system based on the current state and the control inputs applied.

- **Optimization:** the MPC algorithm solves an optimization problem to generate optimal control inputs that minimize a cost function, which is typically defined to achieve a specific mission objective, such as minimizing energy consumption or maximizing accuracy.

- **Implementation:** the MPC algorithm applies the optimal control inputs to the AUV and repeats the prediction and optimization steps at each time step.

The application of MPC for AUV trajectory optimization has been demonstrated in various real-world scenarios such as seabed mapping, underwater inspection, and scientific research. For example, in seabed mapping applications, AUVs equipped with sonar sensors can use MPC to optimize their trajectory to cover the seabed efficiently and accurately [7]. In underwater inspection applications, AUVs equipped with cameras and other sensors can use MPC to optimize their trajectory to inspect underwater structures and pipelines [20]. In scientific research, AUVs equipped with scientific instruments can use MPC to optimize their trajectory to collect oceanographic data such as temperature, salinity, and current profiles [5].

In conclusion, the trajectory optimization of a 6DOF AUV using MPC is a promising technique to improve the performance and efficiency of AUVs in various underwater applications [21]. The MPC algorithm provides a systematic approach to optimize the AUV's trajectory by considering system constraints and disturbances [9]. The application of MPC for AUV trajectory optimization has been demonstrated in various real-world scenarios and has shown promising results [4]. Further research is needed to investigate the limitations and potential of MPC for AUV trajectory optimization in more complex and dynamic underwater environments.

# Chapter 2

# Autonomous Underwater Vehicle

Before getting into the physics of the vehicle, it is necessary to develop a proper understanding of the vehicle that is going to be used. For our study, we have mainly used the Remote Environment Monitoring UnitS (REMUS 100) [20].

We will define the vehicle's physical attribute. This covers several parameters such as vehicle's profile, mass distribution, fin placement, etc, Identifying all these parameters will help better simulate the vehicle's behaviour [20].

## 2.1 REMUS 100

The REMUS 100 takes its name from its maximum operating depth of 100 meters. This study leverages the vehicle model developed by NTNU AUR-lab. See Figure 2.1 for the image of the vehicle. Technical specifications are given in Table 2.1.

### 2.1.1 Weight and Buoyancy of Vehicle

The weight of the REMUS vehicle varies between missions [20]. It depends on the type battery and amount of ballast used. A typical REMUS vehicle

Table 2.1: REMUS 100 Vehicle Physical Attributes

| Parameter | Value | Units | Description |
|---|---|---|---|
| l | 1.60 | $m$ | Vehicle Total Length |
| d | 0.19 | $m$ | Vehicle Cylindrical Diameter |
| h | 100 | $m$ | Maximum Operational Depth |

is ballasted with 0.70 kg so that, in the case of a computer or power failure, it will automatically float to the surface [20]. Typical values for the REMUS weight and buoyancy are given in Table 2.2.

Table 2.2: REMUS Weight and Buoyancy

| Parameter | Value | Units |
|---|---|---|
| $W$ | 304.0 | $N$ |
| $B$ | 311.0 | $N$ |

### 2.1.2 Center of Buoyancy and Center of Gravity

The center of buoyancy of a REMUS remains constant during missions because the hull's exterior is rarely altered. However, it's center of gravity changes since it has to balance itself [20]. Typical values of CG and CB of a REMUS 100 are given in Table 2.3 and Table 2.4.

Table 2.3: Center of Buoyancy wrt Origin at Vehicle Nose

| Parameter | Value | Units |
|---|---|---|
| $x_{cb}$ | -0.61 | $m$ |
| $y_{cb}$ | 0.00 | $m$ |
| $z_{cb}$ | 0.00 | $m$ |

### 2.1.3 Moment of Inertia Matrix Tensor

Moment of inertia is defined with respect to the body-fixed origin of the vehicle. It is located at center of buoyancy. Since the products of inertia

Table 2.4: Center of Gravity wrt Origin at Center of Buoyancy

| Parameter | Value | Units |
|---|---|---|
| $x_{cg}$ | 0.0000 | $m$ |
| $y_{cg}$ | 0.0000 | $m$ |
| $z_{cg}$ | 0.0196 | $m$ |

$I_{xy}$, $I_{xz}$, $I_{yz}$ are small as compared to $I_{xx}$, $I_{yy}$, $I_{zz}$, we can ignore them. We will assume that the center of gravity of the vehicle remains unchanged throughout the mission [20]. Thus, the estimated values of moments of inertia as described in Table 2.5 roughly remains constant throughout the mission.

Table 2.5: Moments of Inertia wrt Origin at Center of Buoyancy

| Parameter | Value | Units |
|---|---|---|
| $I_{xx}$ | 0.177 | $kg.m^2$ |
| $I_{yy}$ | 3.450 | $kg.m^2$ |
| $I_{zz}$ | 3.450 | $kg.m^2$ |


Figure 2.1: REMUS 100 Autonomous Underwater Vehicle [22].

# Chapter 3

# Equation Formulation

In this chapter, we will define various frames of references being used throughout the study. This will be followed by the various aspects of the kinematics and dynamics of the vehicle [20]. The governing equations consist of the following elements:

1. *Kinematics,* which includes the geometric aspect of the motion.
2. *Rigid-body Dynamics,* which describes the vehicle's inertia.
3. *Mechanics,* refers to various types of forces and moments acting on the vehicle body.

Further discussion has been carried out in the following sections.

## 3.1 NED Frame of reference

Our study utilizes the North-East-Down (NED) frame as the default frame of reference [20]. This information can be visualized in greater detail by referring to Figure 3.1. It is important to note that the NED frame is a commonly used convention in various fields, including aviation, navigation, and robotics, due to its simplicity and ease of use [20]. Additionally, it allows for convenient representation of the orientation and position of an object with respect to the Earth's surface.

## 3.2 Body-Fixed Origin Coordinate Frame

Throughout the entire duration of the study, the origin of the vehicle's body-fixed coordinate system is positioned at the center of buoyancy of the vehicle, as specified in Section 2.1.2. It is important to note that this choice of origin has significant implications for the equations of motion, particularly for the calculation of the vehicle's center of gravity and its diagonal inertia tensor [20]. By defining the body-fixed coordinate system in this way, the simplified equations of motion for a rigid body system in six degrees of freedom, as presented in the study by [20], can be derived. Additionally, the assumption that the vehicle's products of inertia are small, as stated in Section 2.1.3, allows for the diagonal inertia tensor to be calculated based on the values of the vehicle's principal moments of inertia.

## 3.3 Vehicle Kinematics

The movement of a body-fixed frame of reference can be described in relation to an inertial or earth-fixed reference frame [20]. To illustrate the vehicle's overall motion in all six degrees of freedom, the following vectors can be employed:

$$\begin{aligned} \boldsymbol{\eta}_1 &= \begin{bmatrix} x & y & z \end{bmatrix}^T; \quad & \boldsymbol{\eta}_2 &= \begin{bmatrix} \phi & \theta & \psi \end{bmatrix}^T \\ \boldsymbol{v}_1 &= \begin{bmatrix} u & v & w \end{bmatrix}^T; \quad & \boldsymbol{v}_2 &= \begin{bmatrix} p & q & r \end{bmatrix}^T \\ \boldsymbol{\tau}_1 &= \begin{bmatrix} X & Y & Z \end{bmatrix}^T; & \boldsymbol{\tau}_2 &= \begin{bmatrix} K & M & N \end{bmatrix}^T \end{aligned} \tag{3.1}$$

in which the vehicle's position and orientation with respect to the earth-fixed reference frame are described by the vector $\boldsymbol{\eta}$, while the vehicle's translational and rotational velocities relative to the body-fixed reference frame are represented by the vector $\boldsymbol{v}$ [20]. Additionally, the total forces and moments exerted on the vehicle relative to the body-fixed reference frame are represented by the vector $\boldsymbol{\tau}$ [20]. Figure 3.1 displays a visual representation of the vehicle coordinate system [20].

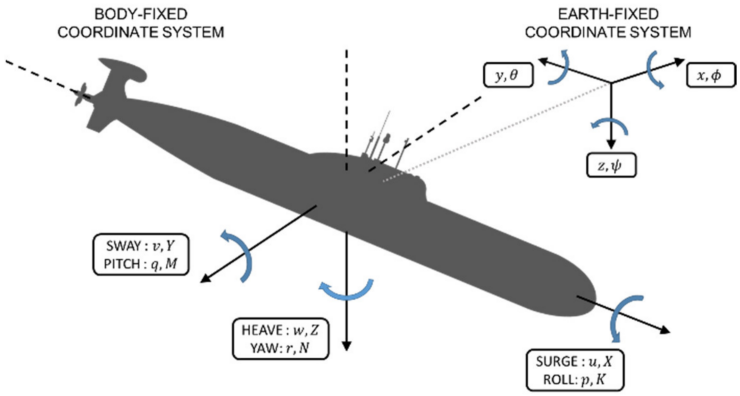


Figure 3.1: Body-Fixed and Inertial Coordinate Frame of Reference for an AUV [23].

The following coordinate transformation can be established to relate the translational velocities of a vehicle in body-fixed and inertial or earth-fixed frames of reference [20]. This transformation is crucial for the understanding and analysis of the motion of a vehicle in three-dimensional space.

$$\begin{bmatrix} \dot{x} \\ \dot{y} \\ \dot{z} \end{bmatrix} = \boldsymbol{T_1}(\boldsymbol{\eta}_2) \begin{bmatrix} u \\ v \\ w \end{bmatrix} \tag{3.2}$$

where

$$\boldsymbol{T}_1(\boldsymbol{\eta}_2) = \begin{bmatrix} \cos\psi\cos\theta & -\sin\psi\cos\phi + \cos\psi\sin\theta\sin\phi & \sin\psi\sin\phi + \cos\psi\sin\theta\cos\phi \\ \sin\psi\cos\theta & \cos\psi\cos\phi + \sin\psi\sin\theta\sin\phi & -\cos\psi\sin\phi + \sin\psi\sin\theta\cos\phi \\ -\sin\theta & \cos\theta\sin\phi & \cos\theta\cos\phi \end{bmatrix} \tag{3.3}$$

is known as the **Transformation Matrix** for translational velocities [18]. Note that $\boldsymbol{T_1}(\boldsymbol{\eta}_2)$ is orthogonal:

$$(\boldsymbol{T_1}(\boldsymbol{\eta}_2))^{-1} = (\boldsymbol{T_1}(\boldsymbol{\eta}_2))^T \tag{3.3}$$

The coordinate transformation serves to establish the connection between rotational velocities of the body-fixed and earth-fixed frames of reference. In

other words, it allows for the description of how the vehicle rotates relative to the earth-fixed frame of reference based on the rotational velocities observed in the body-fixed frame of reference.

$$\begin{bmatrix} \dot{\phi} \\ \dot{\theta} \\ \dot{\psi} \end{bmatrix} = T_2(\boldsymbol{\eta}_2) \begin{bmatrix} p \\ q \\ r \end{bmatrix} \tag{3.4}$$

where

$$T_2(\boldsymbol{\eta}_2) = \begin{bmatrix} 1 & \sin\phi\tan\theta & \cos\phi\tan\theta \\ 0 & \cos\phi & -\sin\phi \\ 0 & \sin\phi/\cos\theta & \cos\phi/\cos\theta \end{bmatrix} \tag{3.5}$$

## 3.4 Vehicle Dynamics

The location of a vehicle's center of gravity (CG) and center of buoyancy (CB) are critical factors that impact its motion and stability. As explained by Limpert et al. [16] and El-Gindy et al. [3], the CG represents the point at which the vehicle's mass is concentrated, while the CB refers to the point at which the buoyancy force of the vehicle is centered. These points are defined in terms of the body-fixed frame of reference, which is the frame of reference fixed to the vehicle's body, rather than the earth-fixed frame of reference. This is important for vehicle kinematics analysis because the movement of the CG and CB relative to the body-fixed frame of reference determines how the vehicle behaves in motion, including its acceleration, deceleration, and turning movements.

$$\boldsymbol{r}_G = \begin{bmatrix} x_g \\ y_g \\ z_g \end{bmatrix} \quad \boldsymbol{r}_B = \begin{bmatrix} x_b \\ y_b \\ z_b \end{bmatrix} \tag{3.6}$$

According to Section 3.2, the origin of the body-fixed frame is situated at the CB. Thus, the simplified equations of motion for a rigid body system in six degrees of freedom, specified in the body-fixed frame of reference, can be expressed as shown in [20]:

$$
\begin{aligned}
m\left[\dot{u} - vr + wq - x_g\left(q^2 + r^2\right) + z_g(pr + \dot{q})\right] &= \sum X_{\text{ext}} \\
m\left[\dot{v} - wp + ur + z_g(qr - \dot{p}) + x_g(qp + \dot{r})\right] &= \sum Y_{\text{ext}} \\
m\left[\dot{w} - uq + vp - z_g\left(p^2 + q^2\right) + x_g(rp - \dot{q})\right] &= \sum Z_{\text{ext}} \\
I_{xx}\dot{p} + \left(I_{zz} - I_{yy}\right)qr + m\left[-z_g(\dot{v} - wp + ur)\right] &= \sum K_{\text{ext}} \\
I_{yy}\dot{q} + \left(I_{xx} - I_{zz}\right)rp + m\left[z_g(\dot{u} - vr + wq) - x_g(\dot{w} - uq + vp)\right] &= \sum M_{\text{ext}} \\
I_{zz}\dot{r} + \left(I_{yy} - I_{xx}\right)pq + m\left[x_g(\dot{v} - wp + ur)\right] &= \sum N_{\text{ext}}
\end{aligned}
\tag{3.8}
$$

Here, $m$ denotes the vehicle mass, and the first three equations signify translational motion while the last three represent rotational motion. [20] As the body-fixed coordinate system of the vehicle is centered at the vehicle CB, the inertia tensor is diagonal, as shown below:

$$
\boldsymbol{I_o} = \begin{bmatrix} I_{xx} & 0 & 0 \\ 0 & I_{yy} & 0 \\ 0 & 0 & I_{zz} \end{bmatrix} \tag{3.7}
$$

This is based on the assumption made in Section 2.1.3 that the vehicle products of inertia are small.

## 3.5 Vehicle Mechanics

The equations of rigid body dynamics for a vehicle consider the external forces and moments acting on it, as shown in Equation 3.8.

$$\sum F_{\text{ext}} = F_{\text{hydrostatic}} + F_{\text{lift}} + F_{\text{drag}} + F_{\text{control}} \tag{3.8}$$

As stated in Hoerner (1965) [14], the vehicle coefficients play a crucial role in determining these external forces and moments. These coefficients are typically a combination of theoretical equations and empirically-derived formulae and can be estimated using various methods, which are outlined in Chapter 4. The accuracy of these coefficients is essential for accurate predictions of the vehicle's behavior and motion.

# Chapter 4

# Estimation of Vehicle Coefficients

In this chapter, we will determine the coefficients that contribute to forces and moments encountered by a REMUS vehicle.

## 4.1 Hydrostatic Forces and Moments

The hydrostatic forces and moments acting on a vehicle result from the interplay between its weight and buoyancy forces. The vehicle's weight can be represented by $W = m \times g$, where $m$ denotes the mass of the vehicle, and $g$ denotes the acceleration due to gravity. On the other hand, the vehicle's buoyancy can be expressed as $B = V\rho g$, where $\rho$ refers to the density of the fluid in which the vehicle is submerged and $V$ denotes the total volume displaced by the vehicle.

To describe these forces and moments in terms of body-fixed coordinates, it is necessary to utilize a transformation matrix, which is presented in Equation ??:

$$\boldsymbol{f}_G(\boldsymbol{\eta}_2) = \boldsymbol{T}_1^{-1} \begin{bmatrix} 0 \\ 0 \\ W \end{bmatrix} \quad \boldsymbol{f}_B(\boldsymbol{\eta}_2) = \boldsymbol{T}_1^{-1} \begin{bmatrix} 0 \\ 0 \\ B \end{bmatrix} \tag{4.1}$$

The hydrostatic forces and moments acting on the vehicle in the body-fixed frame of reference can be expressed as follows:

$$\begin{aligned} \boldsymbol{F}_{hs} &= \boldsymbol{f}_G - \boldsymbol{f}_B \\ \boldsymbol{M}_{hs} &= \boldsymbol{r}_G \times \boldsymbol{f}_G - \boldsymbol{r}_B \times \boldsymbol{f}_B \end{aligned} \tag{4.2}$$

The hydrostatic forces and moments that affect the vehicle while in motion can be described in the body-fixed frame of reference. Expressing these forces and moments mathematically, we use the following equations:

$$\begin{aligned} X_{hs} &= -(W - B)\sin\theta \\ Y_{hs} &= (W - B)\cos\theta\sin\phi \\ Z_{hs} &= (W - B)\cos\theta\cos\phi \\ K_{hs} &= -(y_g W - y_b B)\cos\theta\cos\phi - (z_g W - z_b B)\cos\theta\sin\phi \\ M_{hs} &= -(z_g W - z_b B)\sin\theta - (x_g W - x_b B)\cos\theta\cos\phi \\ N_{hs} &= -(x_g W - x_b B)\cos\theta\sin\phi - (y_g W - y_b B)\sin\theta \end{aligned} \tag{4.3}$$

Note that the hydrostatic moment's opposition to deflections in the pitch and roll directions makes it a stabilizing moment [2].

## 4.2 Hydrodynamic Damping Parameter

The damping of an underwater vehicle moving at a high speed in six degrees of freedom is coupled and highly non-linear [13]. The following assumptions have been made in order to simplify this model [19]:

- We will neglect linear and angular coupled terms, assuming that terms such as $Y_{rv}$ and $M_{rv}$ are relatively small.
- We will assume the vehicle is top-bottom (xy-plane) and port-starboard (xz-plane) symmetric, ignoring the vehicle asymmetry caused by the sonar transducer. This allows us to neglect the drag-induced moments such as $K_{v|v|}$ and $M_{u|u|}$.

- We will neglect any damping terms greater than second-order, allowing us to drop the higher-order terms such as $Y_{vvv}$.

### 4.2.1 Axial Drag Coefficient

The Axial Drag Coefficient describes the resistance an AUV encounters when moving in a specific direction. It considers a number of variables, including the size and shape of the vehicle, the direction and speed of motion, and the characteristics of the fluid medium. The axial drag coefficient depends on the speed, angle of attack, and several other factors of the vehicle. It is a non-linear function and can be expressed by the following axial drag coefficient [11]:

$$X_{u|u|} = -\frac{1}{2}\rho c_{\mathrm{d}} A_f \tag{4.3}$$

where $\rho$ is the density of the surrounding fluid, $A_f$ is the vehicle frontal area, and $c_{\mathrm{d}}$ the axial drag coefficient of the vehicle.

### 4.2.2 Crossflow Drag Coefficient

The total of the hull cross-flow drag and the fin cross-flow drag is the vehicle cross-flow drag. The following formula is used to determine the hull added mass: The sum of the drags on the two-dimensional cylindrical vehicle cross-sections serves as an approximation for the total hull drag. [6].

### 4.2.3 Drag due to Roll

We can approximate the rolling resistance of the vehicle by assuming that the primary component of the rolling resistance of the vehicle is caused by the crossflow drag of the fins. This results in the following equation for the rolling drag coefficient of the vehicle:

$$K_{p|p|} = Y_{vvf} r_{\mathrm{mean}}^3 \tag{4.4}$$

where $Y_{vvf}$ is the fin component of the vehicle crossflow drag coefficient,

and $r_{\text{mean}}$ is the mean fin height above the vehicle centerline. This is at best a rough approximation for the actual value.

## 4.3 Matrix of Added Mass coefficients

The total mass of water that travels with a moving object as it accelerates is referred to as added mass. The added mass matrix of the vehicle for REMUS 100, which has symmetry in the top-bottom and port-starboard directions, can be written as follows:

$$\begin{bmatrix} m_{11} & 0 & 0 & 0 & 0 & 0 \\ 0 & m_{22} & 0 & 0 & 0 & m_{26} \\ 0 & 0 & m_{33} & 0 & m_{35} & 0 \\ 0 & 0 & 0 & m_{44} & 0 & 0 \\ 0 & 0 & m_{53} & 0 & m_{55} & 0 \\ 0 & m_{62} & 0 & 0 & 0 & m_{66} \end{bmatrix} \tag{4.5}$$

which is equivalent to:

$$\begin{bmatrix} X_{\dot{u}} & 0 & 0 & 0 & 0 & 0 \\ 0 & Y_{\dot{v}} & 0 & 0 & 0 & N_{\dot{v}} \\ 0 & 0 & Z_{\dot{w}} & 0 & M_{\dot{w}} & 0 \\ 0 & 0 & 0 & K_{\dot{p}} & 0 & 0 \\ 0 & 0 & Z_{\dot{q}} & 0 & M_{\dot{q}} & 0 \\ 0 & Y_{\dot{r}} & 0 & 0 & 0 & N_{\dot{r}} \end{bmatrix} \tag{4.6}$$

Substituting the assumptions mentioned earlier into the expanded equations for fluid forces and moments allows for the elimination of certain terms. As a result, the following equations can be obtained:

$$
\begin{aligned}
X_{\mathrm{A}} &= X_{\dot{u}}\dot{u} + Z_{\dot{w}}wq + Z_{\dot{q}}q^2 - Y_{\dot{v}}vr - Y_{\dot{r}}\dot{r}^2 \\
Y_{\mathrm{A}} &= Y_{\dot{v}}\dot{v} + Y_{\dot{r}}\dot{r} + X_{\dot{u}}ur - Z_{\dot{w}}wp - Z_{\dot{q}}pq \\
Z_{\mathrm{A}} &= Z_{\dot{w}}\dot{w} + Z_{\dot{q}}\dot{q} - X_{\dot{u}}uq + Y_{\dot{v}}vp + Y_{\dot{r}}rp \\
K_{\mathrm{A}} &= K_{\dot{p}}\dot{p} \\
M_{\mathrm{A}} &= M_{\dot{w}}\dot{w} + M_{\dot{q}}\dot{q} - (Z_{\dot{w}} - X_{\dot{u}})\,uw - Y_{\dot{r}}vp + (K_{\dot{p}} - N_{\dot{r}})\,rp - Z_{\dot{q}}uq \\
N_{\mathrm{A}} &= N_{\dot{v}}\dot{v} + N_{\dot{r}}\dot{r} - (X_{\dot{u}} - Y_{\dot{v}})\,uv + Z_{\dot{q}}wp - (K_{\dot{p}} - M_{\dot{q}})\,pq + Y_{\dot{r}}ur
\end{aligned}
\tag{4.7}
$$

## 4.4 Body Lift Coefficient

When a vehicle travels through water at an angle of attack, the Bernoulli's Theorem predicts that the vehicle body will be lifted. This causes a separation of flow and pressure reduction along the aft, upper portion of the vehicle hull. As a result, a point force is applied at the center of pressure, leading to a reduction in pressure. However, since the center of pressure does not align with the origin of the vehicle-fixed coordinate system, this force creates a pitching moment around the origin.

This pitching moment can have a significant effect on the vehicle's stability and performance in the water, particularly during maneuvers such as turning or accelerating. It is therefore important to understand and account for this pitching moment when designing and operating watercraft. One way to mitigate the pitching moment is to adjust the trim of the vessel, which involves changing the distribution of weight to alter the angle of the hull in the water. Other methods include the use of hydrofoils or other types of lifting surfaces to reduce the angle of attack and minimize the separation of flow. Ultimately, a thorough understanding of the physics of vehicle motion in water is essential for safe and efficient operation of watercraft.

## 4.5 Lift coefficient of Fins

Two sets of fins are used to control the REMUS vehicle's orientation: two horizontal fins known as stern planes and two vertical fins known as rud-

ders. The stern planes and rudder planes are not operated individually or independently of one another since these pairs of fins work together.

Fin lift coefficient $c_L$ is a function of the effective fin angle of attack $\alpha$.

We can separate the equation into the following sets of fin lift coefficients:

$$\begin{aligned} Y_{uu\delta_r} &= -Y_{uvf} = \rho c_{L\alpha} S_{\text{fin}} \\ Z_{uu\delta_s} &= Z_{uwf} = -\rho c_{L\alpha} S_{\text{fin}} \\ Y_{urf} &= -Z_{uqf} = -\rho c_{L\alpha} S_{\text{fin}}\, x_{\text{fin}} \end{aligned} \tag{4.8}$$

and fin moment coefficients:

$$\begin{aligned} M_{uu\delta_s} &= M_{uwf} = \rho c_{L\alpha} S_{\text{fin}} x_{\text{fin}} \\ N_{uu\delta_r} &= -N_{uvf} = \rho c_{L\alpha} S_{\text{fin}} x_{\text{fin}} \\ M_{uqf} &= N_{urf} = -\rho c_{L\alpha} S_{\text{fin}} x_{\text{fin}}^2 \end{aligned} \tag{4.9}$$

where $S_{\text{fin}}$ the fin planform area, $\delta_e$ the effective fin angle in radians, $v_{\text{e}}$ the effective fin velocity, and $x_{\text{fin}}$ the axial position of the fin post in body-referenced coordinates.

## 4.6 Propeller Model

For the REMUS propulsion system, we will utilise a very basic model that regards the propeller as a constant source of thrust and torque.

### 4.6.1 Thrust due to Propellers

The REMUS vehicle can maintain a constant speed of 1.51 m/s(3 knots) when the propeller speed is adjusted to 1500RPM, according to results of numerous sea tests. At this speed, it can be assumed that the vehicle's axial drag and propeller thrust are identical.

$$\begin{aligned} X_{\text{prop}} &= -X_{u|u|} u|u| \\ &= -2.28 X_{u|u|} \end{aligned} \tag{4.10}$$

### 4.6.2 Torque of Propeller

It was noted that the REMUS vehicle was running at a constant speed of 1500RPM with no pitch angle. Under these circumstances, the vehicle maintained an average roll offset $\phi$ of -5.3 degrees ($-9.3 \times 10^{-2}$) radians. Under these steady conditions, it may be assumed that the vehicle's propeller torque corresponds to the hydrostatic roll moment.

$$\begin{aligned} K_{\text{prop}} &= -K_{HS} = (y_g W - y_b B)\cos\theta\cos\phi + (z_g W - z_b B)\cos\theta\sin\phi \\ &= 0.995\,(y_g W - y_b B) - 0.093\,(z_g W - z_b B) \end{aligned} \tag{4.11}$$

## 4.7 Total External Forces and Moments

By combining the coefficient equations that explain the behaviour of the vehicle, we can get a more succinct representation of the forces and moments acting on it. The sum of these moments and forces can be expressed using the following formula:

$$\begin{aligned} \sum X_{\text{ext}} =& X_{hs} + X_{u|u|}u|u| + X_{\dot{u}}\dot{u} + X_{wq}wq + X_{qq}qq + X_{vr}vr + X_{rr}rr \\ &+ X_{\text{prop}} \\ \sum Y_{\text{ext}} =& Y_{hs} + Y_{v|v|}v|v| + Y_{r|r|}r|r| + Y_{\dot{v}}\dot{v} + Y_{\dot{r}}\dot{r} \\ &+ Y_{ur}ur + Y_{wp}wp + Y_{pq}pq + Y_{uv}uv + Y_{uu\delta_r}u^2\delta_r \\ \sum Z_{\text{ext}} =& Z_{hs} + Z_{w|w|}w|w| + Z_{q|q|}q|q| + Z_{\dot{w}}\dot{w} + Z_{\dot{q}}\dot{q} \\ &+ Z_{uq}uq + Z_{vp}vp + Z_{rp}rp + Z_{uw}uw + Z_{uu\delta_s}u^2\delta_s \\ \sum K_{\text{ext}} =& K_{hs} + K_{p|p|}p|p| + K_{\dot{p}}\dot{p} + K_{\text{prop}} \\ \sum M_{\text{ext}} =& M_{hs} + M_{w|w|}w|w| + M_{q|q|}q|q| + M_{\dot{w}}\dot{w} + M_{\dot{q}}\dot{q} \\ &+ M_{uq}uq + M_{vp}vp + M_{rp}rp + M_{uw}uw + M_{uu\delta_s}u^2\delta_s \\ \sum N_{\text{ext}} =& N_{hs} + N_{v|v|}v|v| + N_{r|r|}r|r| + N_{\dot{v}}\dot{v} + N_{\dot{r}}\dot{r} \\ &+ N_{ur}ur + N_{wp}wp + N_{pq}pq + N_{uv}uv + N_{uu\delta_r}u^2\delta_r \end{aligned} \tag{4.13}$$

This concise representation of the dynamics will allow us to more precisely and effectively analyse the behaviour of the vehicle. By considering the various coefficients that affect the forces and moments acting upon the vehicle, we can gain more insight into its performance and identify areas in need of improvement.

The equation described above is therefore a helpful tool in our effort to understand and enhance the behaviour of the vehicle.

Table 1.1: REMUS Non-Linear Force Parameters

| Parameter | Value | Units | Description |
|---|---|---|---|
| $X_{uu}$ | $-1.62$ | kg/m | Cross-flow Drag |
| $X_{\dot{u}}$ | $-0.930$ | kg | Added Mass |
| $X_{wq}$ | $-35.5$ | kg/rad | Added Mass Cross-term |
| $X_{qq}$ | $-1.93$ | kg $\cdot$ m/rad | Added Mass Cross-term |
| $X_{vr}$ | $+35.5$ | kg/rad | Added Mass Cross-term |
| $X_{rr}$ | $-1.93$ | kg $\cdot$ m/rad | Added Mass Cross-term |
| $X_{prop}$ | $+3.86$ | N | Propeller Thrust |
| $Y_{vv}$ | $-131$ | kg/m | Cross-flow Drag |
| $Y_{rr}$ | $+0.632$ | kg $\cdot$ m/rad | Cross-flow Drag |
| $Y_{uv}$ | $-28.6$ | kg/m | Body Lift Force and Fin Lift |
| $Y_{\dot{v}}$ | $-35.5$ | kg | Added Mass |
| $Y_{\dot{r}}$ | $+1.93$ | kg $\cdot$ m/rad | Added Mass |
| $Y_{ur}$ | $+5.22$ | kg/rad | Added Mass Cross Term and Fin Lift |
| $Y_{wp}$ | $+35.5$ | kg/rad | Added Mass Cross-term |
| $Y_{pq}$ | $+1.93$ | kg $\cdot$ m/rad | Added Mass Cross-term |
| $Y_{uudr}$ | $+9.64$ | kg/(m $\cdot$ rad) | Fin Lift Force |
| $Z_{ww}$ | $-131$ | kg/m | Cross-flow Drag |
| $Z_{qq}$ | $-0.632$ | kg $\cdot$ m/rad | Cross-flow Drag |
| $Z_{uw}$ | $-28.6$ | kg/m | Body Lift Force and Fin Lift |
| $Z_{\dot{w}}$ | $-35.5$ | kg | Added Mass |
| $Z_{\dot{q}}$ | $-1.93$ | kg $\cdot$ m/rad | Added Mass |
| $Z_{uq}$ | $-5.22$ | kg/rad | Added Mass Cross-term and Fin Lift |
| $Z_{vp}$ | $-35.5$ | kg/rad | Added Mass Cross-term |
| $Z_{rp}$ | $+1.93$ | kg/rad | "Added Mass Cross-term" |
| $Z_{uuds}$ | $-9.64$ | kg/(m $\cdot$ rad) | Fin Lift Force |

Table 1.2: REMUS Non-Linear Moment Parameters

| Parameter | Value | Units | Description |
|---|---|---|---|
| $K_{pp}$ | $-0.0013$ | $\text{kg} \cdot \text{m}^2/\text{rad}^2$ | Rolling Resistance |
| $K_{\dot{p}}$ | $-0.014$ | $\text{kg} \cdot \text{m}^2/\text{rad}$ | Added Mass |
| $K_{prop}$ | $-0.543$ | $\text{N} \cdot \text{m}$ | Propeller Torque |
| $M_{ww}$ | $+3.18$ | kg | Cross-flow Drag |
| $M_{qq}$ | $-9.40$ | $\text{kg} \cdot \text{m}^2/\text{rad}^2$ | Cross-flow Drag |
| $M_{uw}$ | $+24.0$ | kg | Body and Fin Lift and Munk Moment |
| $M_{\dot{w}}$ | $-1.$ | $\text{kg} \cdot \text{m}$ | Added Mass |
| $M_{\dot{q}}$ | $-4.88$ | $\text{kg} \cdot \text{m}^2/\text{rad}$ | Added Mass |
| $M_{uq}$ | $-2.00$ | $\text{kg} \cdot \text{m}/\text{rad}$ | Added Mass Cross Term and Fin Lift |
| $M_{vp}$ | $-1.93$ | $\text{kg} \cdot \text{m}/\text{rad}$ | Added Mass Cross Term |
| $M_{rp}$ | $+4.86$ | $\text{kg} \cdot \text{m}^2/\text{rad}^2$ | Added Mass Cross-term |
| $M_{uuds}$ | $-6.15$ | kg/rad | Fin Lift Moment |
| $N_{vv}$ | $-3.18$ | kg | Cross-flow Drag |
| $N_{rr}$ | $-9.40$ | $\text{kg} \cdot \text{m}^2/\text{rad}^2$ | Cross-flow Drag |
| $N_{uv}$ | $-24.0$ | kg | Body and Fin Lift and Munk Moment |
| $N_{\dot{v}}$ | $+1.93$ | $\text{kg} \cdot \text{m}$ | Added Mass |
| $N_{\dot{r}}$ | $-4.88$ | $\text{kg} \cdot \text{m}^2/\text{rad}$ | Added Mass |
| $N'_{ur}$ | $-2.00$ | $\text{kg} \cdot \text{m}/\text{rad}$ | Added Mass Cross Term and Fin Lift |
| $N_{wp}$ | $-1.93$ | $\text{kg} \cdot \text{m}/\text{rad}$ | Added Mass Cross Term |
| $N_{pq}$ | $-4.86$ | $\text{kg} \cdot \text{m}^2/\text{rad}^2$ | Added Mass Cross-term |
| $N_{uudr}$ | $-6.15$ | kg/rad | Fin Lift Moment |

## 4.8 Combined 6DOF Equations of Motions

We can derive a unified set of non-linear equations of motion that accurately capture the behavior of the REMUS vehicle across all six degrees of freedom by combining the equations describing the rigid-body dynamics of the vehicle with those governing the forces and moments acting upon it.

This set of equations offers a thorough representation of the dynamics of the vehicle, enabling us to precisely model and examine its motion. We can better understand the behavior of the vehicle and create more efficient control strategies to enhance its performance by taking into account the intricate interplay of forces and moments that affect the trajectory of the vehicle.

As a result, we now give the REMUS vehicle's resulting non-linear equations of motion:

Surge, or translation along the x-axis:

$$\begin{aligned} m\left[\dot{u} - vr + wq - x_g\left(q^2 + r^2\right) + y_g(pq - \dot{r}) + z_g(pr + \dot{q})\right] = \\ X_{hs} + X_{u|u|}u|u| + X_{\dot{u}}\dot{u} + X_{wq}wq + X_{qq}qq \\ +X_{vr}vr + X_{rr}rr + X_{\text{prop}} \end{aligned} \tag{4.12}$$

Sway, or translation along the y-axis:

$$\begin{aligned} m\left[\dot{v} - wp + ur - y_g\left(r^2 + p^2\right) + z_g(qr - \dot{p}) + x_g(qp + \dot{r})\right] = \\ Y_{hs} + Y_{v|v|}v|v| + Y_{r|r|}r|r| + Y_{\dot{v}}\dot{v} + Y_{\dot{r}}\dot{r} \\ +Y_{ur}ur + Y_{wp}wp + Y_{pq}pq + Y_{uv}uv + Y_{uu\delta_r}u^2\delta_r \end{aligned} \tag{4.13}$$

Heave, or translation along the z-axis:

$$\begin{aligned} m[\dot{w} - uq + vp - z_g\left(p^2 + q^2\right) + x_g(rp - \dot{q}) + y_g(rq + \dot{p})\big] = \\ Z_{hs} + Z_{w|w|}w|w| + Z_{q|q|}q|q| + Z_{\dot{w}}\dot{w} + Z_{\dot{q}}\dot{q} \\ + Z_{uq}uq + Z_{vp}vp + Z_{rp}rp + Z_{uw}uw + Z_{uu\delta_s}u^2\delta_s \end{aligned} \tag{4.14}$$

Roll, or rotation about the $x$-axis:

$$\begin{aligned} I_{xx}\dot{p} + (I_{zz} - I_{yy})\,qr + m\left[y_g(\dot{w} - uq + vp) - z_g(\dot{v} - wp + ur)\right] = \\ K_{hs} + K_{p|p|}p|p| + K_{\dot{p}}\dot{p} + K_{\text{prop}} \end{aligned} \tag{4.15}$$

Pitch, or rotation about the y-axis:

$$\begin{aligned} I_{yy}\dot{q} + (I_{xx} - I_{zz})\,rp + m\left[z_g(\dot{u} - vr + wq) - x_g(\dot{w} - uq + vp)\right] = \\ M_{hs} + M_{w|w|}w|w| + M_{q|q|}q|q| + M_{\dot{w}}\dot{w} + M_{\dot{q}}\dot{q} \\ +M_{uq}uq + M_{vp}vp + M_{rp}rp + M_{uw}uw + M_{uu\delta_s}u^2\delta_s \end{aligned} \tag{4.16}$$

Yaw, or rotation about the z-axis:

$$\begin{aligned} I_{zz}\dot{r} + (I_{yy} - I_{xx})\,pq + m\left[x_g(\dot{v} - wp + ur) - y_g(\dot{u} - vr + wq)\right] = \\ N_{hs} + N_{v|v|}v|v| + N_{r|r|}r|r| + N_{\dot{v}}\dot{v} + N_{\dot{r}}\dot{r} \\ +N_{ur}ur + N_{wp}wp + N_{pq}pq + N_{uv}uv + N_{uu\delta_r}u^2\delta_r \end{aligned} \tag{4.17}$$

The vehicle equations of motion can be condensed once the acceleration terms have been separated from the other terms. This will allow us to comprehend the system's fundamental dynamics with greater clarity.

We can efficiently write the forces and accelerations that controls the vehicle's behavior by organizing the equations into a matrix. With the help of this matrix representation, we can examine how the system reacts to various inputs and disturbances and create control plans that enhance its functionality.

Consequently, the equations of motion can be written below in matrix form:

$$\begin{bmatrix} \dot{u} \\ \dot{v} \\ \dot{w} \\ \dot{p} \\ \dot{q} \\ \dot{r} \end{bmatrix} = \begin{bmatrix} m - X_{\dot{u}} & 0 & 0 & 0 & mz_g & -my_g \\ 0 & m - Y_{\dot{v}} & 0 & -mz_g & 0 & mx_g - Y_{\dot{r}} \\ 0 & 0 & m - Z_{\dot{w}} & my_g & -mx_g - Z_{\dot{q}} & 0 \\ 0 & -mz_g & my_g & I_{xx} - K_{\dot{p}} & 0 & 0 \\ mz_g & 0 & -mx_g - M_{\dot{w}} & 0 & I_{yy} - M_{\dot{q}} & 0 \\ -my_g & mx_g - N_{\dot{v}} & 0 & 0 & 0 & I_{zz} - N_{\dot{r}} \end{bmatrix}^{-1} \begin{bmatrix} \sum X \\ \sum Y \\ \sum Z \\ \sum K \\ \sum N \\ \sum N \end{bmatrix} \tag{4.18}$$

## 4.9 Linearized Equations of motions

We will proceed to incorporate the controller input into our analysis after deriving the complete set of equations of motion that account for all six degrees of freedom. As a result, we will be able to create the final non-linear equation of motion with control vector, which will give us a more thorough understanding of the behavior of the system.

We will use a body-fixed frame of reference to more conveniently express the non-linear equations. With this frame of reference, we can write the equations more succinctly and intuitively, which will make it easier to analyze and interpret the outcomes.

As a result, the non-linear equations of motion can be expressed as follows in the body-fixed frame of reference:

$$\begin{aligned} \boldsymbol{M\dot{v} + C(v)v + D(v)v + g(\eta) = \tau} \\ \boldsymbol{\dot{\eta} = T_1(\eta_2)v} \end{aligned} \tag{4.19}$$

where

$\boldsymbol{\eta} = \begin{bmatrix} \boldsymbol{x} & \boldsymbol{y} & \boldsymbol{z} & \boldsymbol{\phi} & \boldsymbol{\theta} & \boldsymbol{\psi} \end{bmatrix}^{\boldsymbol{T}}$ is the position vector in earth-fixed reference frame,
$\boldsymbol{M} = \boldsymbol{M_{RB}} + \boldsymbol{M_A}$ is the Total Inertial Mass matrix,
$\boldsymbol{v} = \begin{bmatrix} \boldsymbol{u} & \boldsymbol{v} & \boldsymbol{w} & \boldsymbol{p} & \boldsymbol{q} & \boldsymbol{r} \end{bmatrix}^{\boldsymbol{T}}$ is the velocity vector in body-fixed frame of reference, and
$\boldsymbol{C(v), D(v), g(v)}$ are the Coriolis and Centripetal Force matrix, Damping Force matrix, and Restoring Force matrix respectively.

# Chapter 5

# Model Predictive Control

Trajectory optimization is a crucial task because of which the use of underwater vehicles have increased rapidly these days as compared to their counterpart, Remotely Operated Vehicles (ROVs) [24]. The objective is to generate the optimal path while taking into consideration the vehicle dynamics, environmental conditions, and vehicle energy efficiency. Model Predictive Control (MPC) is a control strategy that has recently become popular for trajectory optimization problems in AUVs.

## 5.1 Overview

Model Predictive Control (MPC) reflects human behaviour whereby we select control actions which we think will lead to the best predicted outcome (or output) over some limited horizon [9]. We constantly update our decisions as new observations become available. Model predictive control (MPC) is a control strategy used to optimize the performance of a dynamic system subject to constraints on the system variables. The basic idea of MPC is to use a model of the system to predict its future behavior and then compute a control input that minimizes a cost function while satisfying the constraints. This cost function typically includes terms that penalize deviations from desired set points, control effort, and violation of constraints.

## 5.2 Trajectory Optimization Problem for AUVs

**Running (stage) Costs:** Characterization of the control objective-

$$\ell(\mathbf{x}, \mathbf{u}) = \|\mathbf{x_u} - \mathbf{x}^r\|^2_{\mathbf{Q}} + \|\mathbf{u} - \mathbf{u}^r\|^2_{\mathbf{R}} \tag{5.1}$$

**Cost Function:** Evaluation of the running costs along the whole prediction horizon-

$$J_N(\mathbf{x}, \mathbf{u}) = \sum_{k=0}^{N-1} \ell\left(\mathbf{x_u}(k), \mathbf{u}(k)\right) \tag{5.2}$$

**Optimal Control Problem (OCP):** Finding a minimizing control sequence-

$$\begin{aligned} \underset{\mathbf{u}}{\text{minimize}}\ & J_N\left(\mathbf{x}_0, \mathbf{u}\right) = \sum_{k=0}^{N-1} \ell\left(\mathbf{x_u}(k), \mathbf{u}(k)\right) \\ \text{subject to } & \mathbf{x_u}(k+1) = \mathbf{f}\left(\mathbf{x_u}(k), \mathbf{u}(k)\right) \\ & \mathbf{x_u}(0) = \mathbf{x}_0, \\ & \mathbf{u}(k) \in U, \quad \forall k \in [0, N-1] \\ & \mathbf{x_u}(k) \in X, \quad \forall k \in [0, N] \end{aligned} \tag{5.3}$$

**Value Function:** Minimum value of the cost function-

$$V_N(\mathbf{x}) = \min_{\mathbf{u}} J_N\left(\mathbf{x}_0, \mathbf{u}\right) \tag{5.4}$$

The trajectory optimization problem for AUVs can be formulated as a dynamic optimization problem where the objective is to find the optimal path that minimizes a given cost function subject to system dynamics and constraints. The cost function can be designed to account for various factors such as energy consumption, time to complete the mission, and environmental factors such as currents and obstacles.

Let $x_k \in \mathbb{R}^n$ be the state of the AUV at time $t_k$, $u_k \in \mathbb{R}^m$ be the control input, $y_k \in \mathbb{R}^p$ be the output, and $d_k \in \mathbb{R}^q$ be the disturbance input. The system dynamics can be described by the following discrete-time model:

$$x_{k+1} = f(x_k, u_k, d_k) \tag{5.5}$$

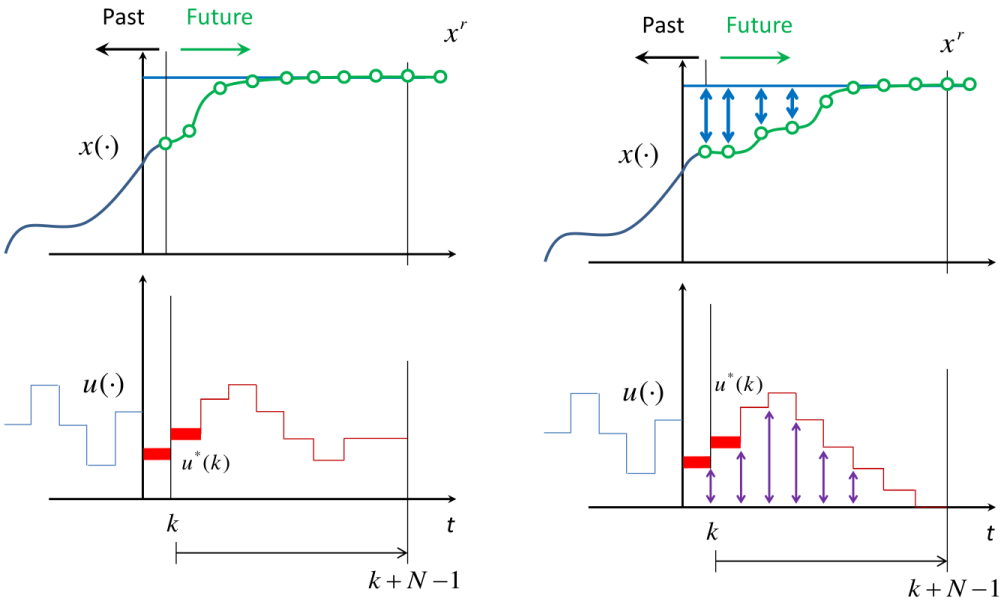


(a) MPC 1 (b) MPC 2

Figure 5.1: Optimization of the output $x(\cdot)$ based on control input $u(\cdot)$ at each timestep. [8]

where $f$ is a nonlinear function. The control input $u_k$ is subject to constraints such as input limits and environmental factors [8]. The objective is to find the optimal control sequence $U^{=}u_0^{,}u_1^{,}\ldots,u_{N-1}$ over a finite horizon $[t_k, t_k + T]$ that minimizes the cost function:

$$J(U) = \sum_{k=0}^{N-1} L(x_k, u_k) + M(x_N) \tag{5.6}$$

where $L$ is the stage cost function, and $M$ is the terminal cost function. The stage cost function can be designed to account for various factors such as energy consumption, time to complete the mission, and environmental factors such as currents and obstacles [8]. The terminal cost function can be designed to ensure that the AUV reaches the desired state at the end of the horizon.

The trajectory optimization problem subject to constraints can be formulated as:

$$\begin{aligned} \underset{U}{\text{minimize}} \quad & J(U) \\ \text{subject to} \quad & x_{k+1} = f(x_k, u_k, d_k), \quad k = 0, \ldots, N-1 \\ & g(x_k, u_k, d_k) \leq 0, \quad k = 0, \ldots, N-1 \\ & h(x_N) \leq 0 \\ & x_0 = x(t_k) \end{aligned} \tag{5.7}$$

# Chapter 6

# Results

Real-time simulations have been performed in order to validate the working of our designed model predictive controller. We demonstrated that the approach works for obstacle avoidance, trajectory optimization task in case of a 2D flow field.

We also carried out simulations for a 3D flow field closely resembling to that of a real-time ocean environment. We used a python based underwater vehicle simulator [22] to validate our results. It uses a Depth-Heading based controller to navigate through the ocean environment.

Complete numerical simulation in presence of different conditions have been carried out in the following sections. All the results are generated in python environment.

## 6.1 Depth Heading control in 3D flow field

The Python Vehicle Simulator was used for simulation of 6 degree of freedom REMUS 100 Underwater Vehicle. The Depth Heading controller uses a Single Input Singel Output (SISO) PID pole placement controller [15].

The REMUS 100 vehicle was given a desired depth of $80m$, and a desired heading of 30 deg. The ocean current speed was $0.5m/sec$ at an angle of 120 deg to the vehicle.

The results are in the form of various states of the vehicle. The controller

outputs are also shown as actuator outputs.

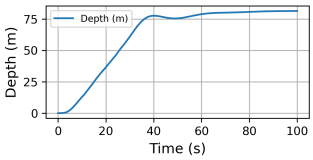


Figure 6.1: Depth

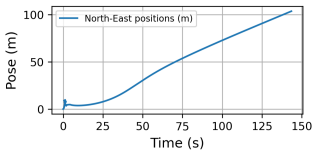


Figure 6.2: Position of vehicle in NED frame.

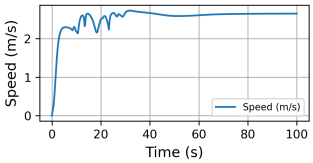


Figure 6.3: Speed

The vehicle starts from origin and acquires a depth as described in the initial configuration 6.1. See Figure 6.1 for the plot of depth of the vehicle.

It starts from origin and headed in the North-East direction because of the set default coordinate frame of reference 3.1. The plot is shown here as follows 6.2.

Maximum speed of a REMUS 100 vehicle is approximately 5 *knots* or 9.8 $km/hr$. The speed of the vehicle as a function of time is shown in Figure 6.3.

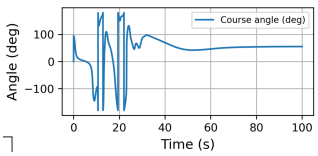


Figure 6.4: Course

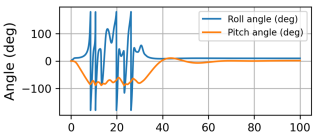


Figure 6.5: Roll Pitch angle

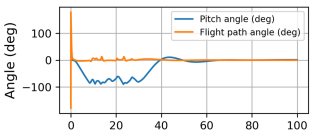


Figure 6.6: Pitch flight path angle

Desired heading of the vehicle is 30 deg East from North 6.1. The course over ground of the vehicle is the direction of heading of the vehicle. It is shown in Figure 6.5.

The roll and pitch angle of the vehicle for the entire mission can be seen in the Figure 6.5 and Figure 6.6. The flight of the vehicle as described in Figure 6.6 is actual direction of motion.

The vehicle Surge, Sway and Heave motion are plotted in Figure 6.7. Initially, as the vehicle is approaching the desired depth it's surge velocity is high and later as time increases it stabilizes it's motion and attains a steady state.

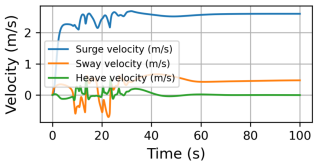


Figure 6.7: Surge, Sway, Heave Velocity

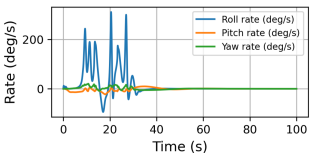


Figure 6.8: Roll, Pitch, Yaw Rate

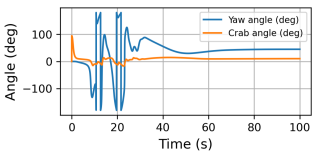


Figure 6.9: Yaw Angle and Crab Angle

The vehicle roll, pitch and yaw rates are shown in Figure 6.8. Because of the presence of turbulence as a result of ocean flow, we can see that there are lot of fluctuations in roll angle rate. This is due to ocean currents angle of attack of the vehicle.

**Crab angle** is the desired angle of heading of an underwater vehicle during its mission so as counter the crossflow drag forces and moments [25]. A plot for the yaw angle as compared to the crab angle of the vehicle is shown in Figure 6.9.

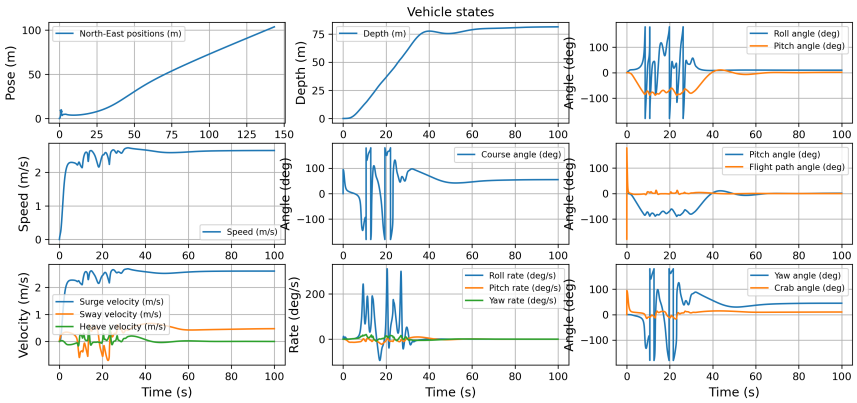


Figure 6.10: Combined description of states of REMUS 100 vehicle obtained with the use of Python Vehicle Simulator [22].

A cumulative plot combining vehicle states and control outputs have been displayed in Figure 6.10.

## 6.2 Obstacle avoidance and trajectory optimization in 2D flow field

The simulation was carried out for a total of 10000 time steps at an interval of 0.01. The total simulation time was 100 seconds. The vehicle was at rest initially. Upon start of simulation, it was introduced to a 2-dimensional time-varying field.

Following scenarios were analysed-

1. Motion in a periodically varying flow field in presence of an obstacle. Refer to Figure 6.12 and 6.13.
2. Optimization of trajectory in presence of a 2D obstacle and no flow fields. Refer to Figure 6.11
3. Trajectory optimization and obstacle avoidance in presence a time varying flow field along with a 2D obstacle. Refer to Figure 6.14 and 6.15.

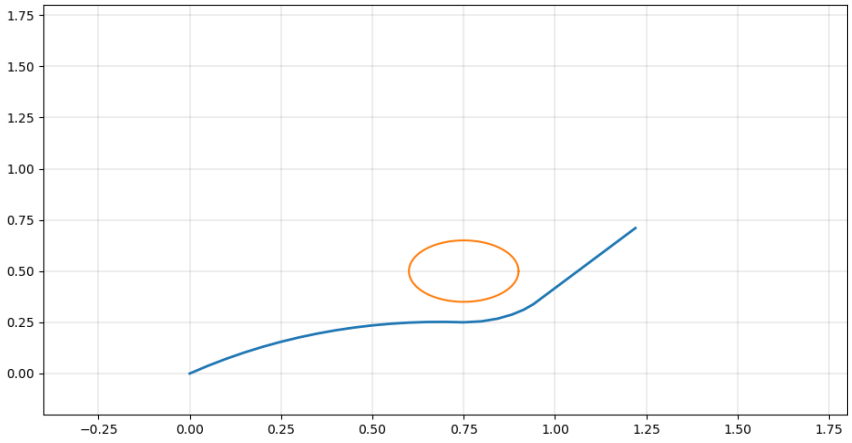


Figure 6.11: Trajectory optimization in presence of 2D obstacle.

First of all, a 2D obstacle was introduced in order to check the trajectory prediction and obstacle avoidance feature of the MPC controller. The obstacle is a 2D circle centered at $(0.75, 0.25)$ with a radius of 0.15 units 6.11.

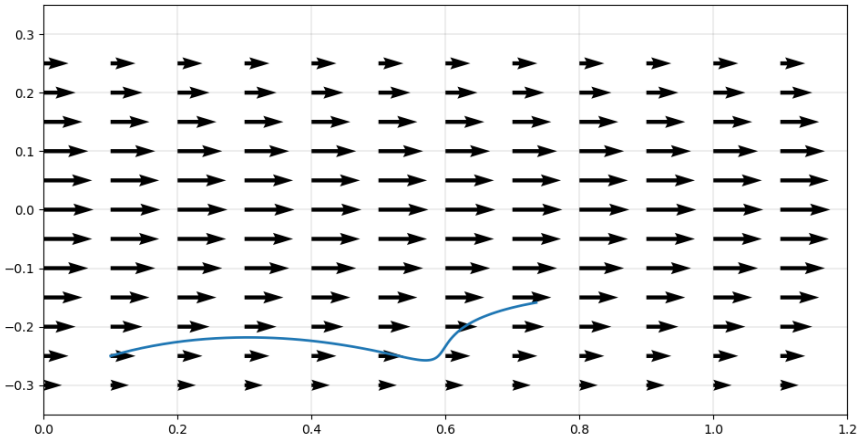


Figure 6.12: Path planning in presence of periodically time varying flow field.

A time varying flow field was introduced which changes it's direction of flow each second 6.12. The controller was given the target location and the task was to reach the target in presence of the flow. It can be seen that the flow field direction opposite to that of motion as a result of this the vehicle changes it's course temporarily to counteract the flow field action 6.13.

An obstacle was placed at the location $(0.75, 0.5)$ and the target was set at $(1.8, 0.8)$. See Figure 6.14. This time a cross flow field was introduced which is curl based motion of the ocean water. This was done to resemble the actual ocean environment. The vehicle is seen to have followed the flow direction to reach the target. Check Figure 6.15 for plot.

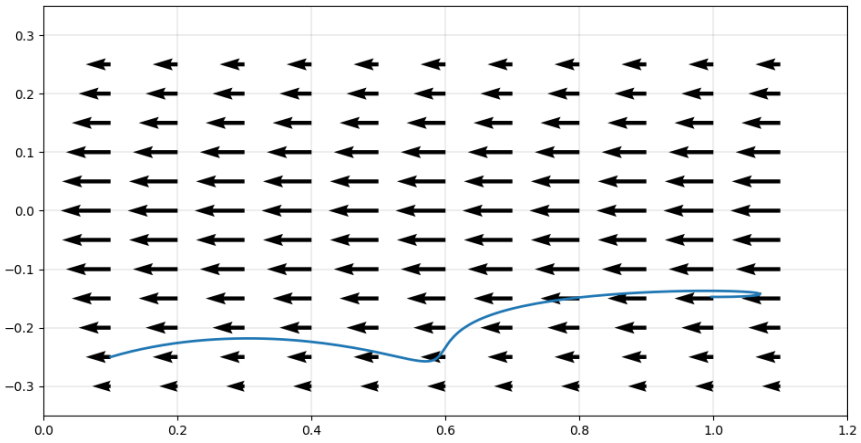


Figure 6.13: Impact of time varying flow field in Trajectory Optimization.

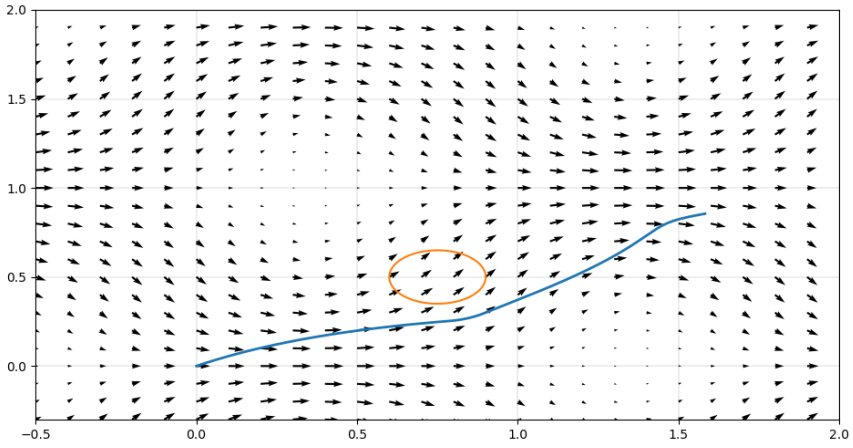


Figure 6.14: Trajectory optimization in presence of 2D obstacle as well as time varying flow field.

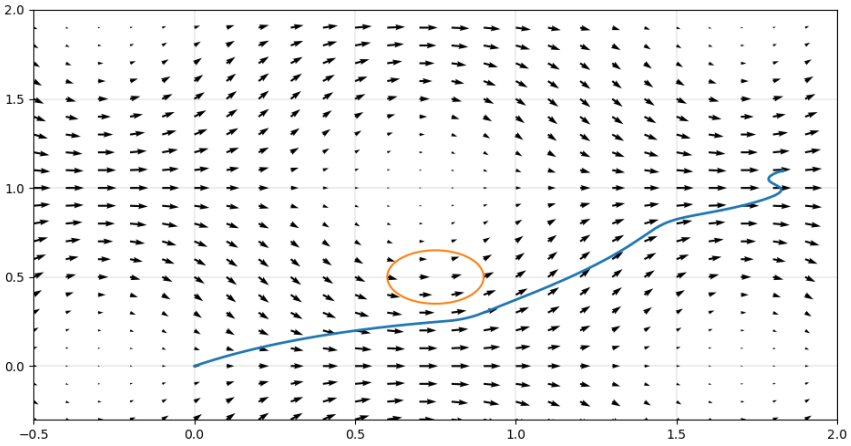


Figure 6.15: Trajectory optimization in presence of 2D obstacle as well as time varying flow field after some time elapsed.

# Chapter 7

# Conclusions

In this thesis, we studied the mechanics of a rigid mass body. We formulated the 6 DoF ewuations of motion of an AUV. We studied about the forces acting on it without the presence of any external forces or inside the ocean water. After that we developed the equations of a rigid body in presence of ideal ocean fluid, this gave us a broad overview of the forces being experienced by the vehicle inside an ideal fluid. We then further move onto extending this model to real fluid. This made us realize the extent of non-linearity and complexity involved in the study of 6 DoF model in presence of real fluid. Further we proceed onto designing a MPC controller which can predict the optimal trajectory from a source to target destination in definite horizon estimate. This controller is used to generate optimal paths for an Underwater Vehicle in presence of real fluid forces.

## 7.1 Observations

In the study of Optimal trajectory optimization of AUV in ocean fluiod particle using MPC, the non-linearity of the 6DoF equations of motions have been observed to be very difficult to handle. Linearizing the equations helped us to a great extent in handling the equations and implementing it further for numerical simulations.

## 7.2 Applications

The study that has been carried out in this thesis has many future applications. One potential application is in underwater surveying and inspection tasks, where accurate and efficient movement of the AUV is crucial for obtaining high-quality data. MPC-based trajectory optimization can help the AUV navigate through complex underwater environments and avoid obstacles while optimizing the trajectory for minimizing energy consumption and travel time. Another application is in underwater search and rescue operations, where time is of the essence, and the ability to navigate through challenging underwater terrain is crucial. Optimal trajectory optimization can enable the AUV to navigate through tight spaces and complex environments while optimizing the search strategy. Additionally, in underwater exploration tasks, such as mapping uncharted regions of the ocean, MPC-based trajectory optimization can help the AUV navigate through unknown environments and adapt its trajectory to changing conditions in real-time. Overall, optimal trajectory optimization of 6 DOF AUVs using MPC has a broad range of potential applications in underwater robotics, making it a promising field for future research and development.

## 7.3 Future Works

There are many emerging areas in this line of work that is yet to be delved into. One such task is to use a deep learning based automatic cost function generation for the MPC which can take into account all the constraints and hence, be able to minimize the objective function.

There are several potential areas for future research on optimal trajectory optimization of 6 Degree Of Freedom (DOF) Autonomous Underwater Vehicle (AUV) using Model Predictive Control (MPC). One potential avenue is to explore the use of deep reinforcement learning (DRL) algorithms to optimize the AUV trajectory in real-time. DRL algorithms can learn from past experiences and adapt their behavior to changing environments, making them well-suited for complex and dynamic underwater environments.

Another area for future research is to investigate the use of multi-objective optimization techniques to optimize the trajectory of the AUV for multiple objectives, such as minimizing energy consumption, travel time, and path deviation. Additionally, there is potential to develop more accurate fluid models and incorporate them into the trajectory optimization framework to improve the accuracy of the predicted trajectories. Finally, there is a need for extensive experimental validation of the trajectory optimization algorithms to ensure their efficacy and robustness in real-world scenarios. Overall, these areas of research have the potential to further advance the field of underwater robotics and enhance the capabilities of AUVs for a broad range of applications, including environmental monitoring, underwater exploration, and search and rescue operations.

# Bibliography


[1] Shahab Heshmati-Alamdari, Alexandros Nikou, and Dimos V. Dimarogonas. Robust trajectory tracking control for underactuated autonomous underwater vehicles in uncertain environments. *IEEE Transactions on Automation Science and Engineering*, 18(3):1288–1301, 2021.

[2] Robert D. Blevins. *Formula for Natural Frequency and Mode shapes*. 2001.

[3] Moustafa El-Gindy and Mahmoud Haddara. Buoyancy determination of waterborne vehicles: a review. *Ocean Engineering*, 126:114–130, 2016.

[4] Muhammad Khalid and Andrey V Savkin. A model predictive control approach to the problem of wind power smoothing with controlled battery storage. *Renewable Energy*, 35(7):1520–1526, 2010.

[5] Paolo Falcone, Manuela Tufo, Francesco Borrelli, Jahan Asgari, and H Eric Tseng. A linear time varying model predictive control approach to the integrated vehicle dynamics control problem in autonomous systems. In *2007 46th IEEE Conference on Decision and Control*, pages 2980–2985. IEEE, 2007.

[6] Thor. I. Fossen. Guidance and control of ocean vehicles. 1999.

[7] Jesus Felez, Yeojun Kim, and Francesco Borrelli. A model predictive control approach for virtual coupling in railways. *IEEE Transactions on Intelligent Transportation Systems*, 20(7):2728–2739, 2019.

[8] Mohamed Mehrez. Optimization based solutions for control and state estimation in dynamical systems (implementation to mobile robots) a workshop, 01 2019.

[9] Robert H. Bishop. *Model-Based Predictive Control: A Practical Approach. CONTROL SERIES*. University of Texas, Austin, Texas, US, 2004.

[10] Alessandra Parisio, Evangelos Rikos, and Luigi Glielmo. A model predictive control approach to microgrid operation optimization. *IEEE Transactions on Control Systems Technology*, 22(5):1813–1827, 2014.

[11] Thor I. Fossen. *Handbook of Marine Craft Hydrodynamics and Motion Control*. John Wiley  Sons, Ltd, 4 2011.

[12] Thor I. Fossen. *Handbook of Marine Craft Hydrodynamics and Motion Control*. Wiley, 2nd edition, April 2021.

[13] Andrew Lammas, Karl Sammut, and Fangpo He. *6-DoF Navigation Systems for Autonomous Underwater Vehicles*. InTech, 3 2010.

[14] Sighard F. Hoerner. *Fluid Dynamic Lift*. 1998.

[15] Saibal Manna, Shaili Shaw, and Ashok Kumar Akella. Design of higher-order regulator system using pole-placement technique. In *2020 International Conference on Computational Intelligence for Smart Power System and Sustainable Energy (CISPSSE)*, pages 1–4, 2020.

[16] Rudolf Limpert and Hans-Joachim Besserer. *Fundamentals of Vehicle Dynamics*. Springer Nature, 2nd edition, 2019.

[17] Markus Maurer, J. Christian Gerdes, Barbara Lenz, and Hermann Winner. *Autonomous Driving: Technical, Legal and Social Aspects*. Springer, 2019.

[18] A J Healey. Dynamics and control of marine robotic vehicles, 2019.

[19] Newman J. N. *Marine Hydrodynamics*. 2018.

[20] Timothy Prestero. Verification of a six-degree of freedom simulation model for the remus autonomous underwater vehicle.

[21] Yongding Zhang, Xiaofeng Liu, Minzhou Luo, and Chenguang Yang. Mpc-based 3-d trajectory tracking for an autonomous underwater vehicle with constraints in complex ocean environments. *Ocean Engineering*, 189:106309, 2019.

[22] Cybergalactic. Python vehicle simulator.

[23] Hyun-Hee Kim, Min Cheol Lee, Hyeon-Jin Cho, Jun-Ho Hwang, and Jong-Seob Won. Smcspo-based robust control of auv in underwater environments including disturbances. *Applied Sciences*, 11(22):10978, Nov 2021.

[24] J. A. Rossiter. *Model-based predictive control : a practical approach*. CRC Press, 2003.

[25] Thor I. Fossen. An adaptive line-of-sight (alos) guidance law for path following of aircraft and marine craft. *IEEE Transactions on Control Systems Technology*, pages 1–8, 2023.